ELSEVIER

Coastal Engineering 40 (2000) 183–206

COASTAL ENGINEERING

www.elsevier.com/locate/coastaleng

Empirical formula for breakage of Dolosse and Tetrapods

H.F. Burcharth [a], K. d'Angremond [b], J.W. van der Meer [c,1], Z. Liu [a,*]

[a] *Department of Civil Engineering, Aalborg University, Sohngaardsholmsvej 57, 9000 Aalborg, Denmark*
[b] *Delft University of Technology, P.O. Box 5048, 2600 GA Delft, Netherlands*
[c] *Delft Hydraulics, P.O. Box 177, 2600 GA Delft, Netherlands*

Received 28 April 1999; accepted 1 March 2000

Abstract

The slender, complex types of armour units, such as Tetrapods and Dolosse are widely used for rubble mound breakwaters. Many failures of such breakwaters were caused by unforeseen early breakage of the units, thus revealing an inbalance between the strength (structural integrity) of the units and the hydraulic stability (resistance to displacements) of the armour layers. Breakage occurs when the stresses from the static, pulsating and impact loads exceeds the tensile strength of the concrete.

While the hydraulic stability can be studied in Froude-scale hydraulic model tests, it is not possible to study armour unit stresses in small scale models. This is partly because the strain in model armour units are too small to be recorded, and partly because the scaling law for impact load generated stresses is nonlinear.

The paper discusses the scaling laws related to type of stresses and presents a method which allows studies of armour unit stresses by means of a load-cell technique. The technique necessitates impact load response calibration of the load-cell mounted model armour units against the equivalent response of prototype or large scale armour units. The procedure followed was presented by Burcharth and Liu (Burcharth, H.F., Liu, Z., 1992. Design of Dolos armour units. In: Proceedings of the 23rd International Conference on Coastal Engineering, Venice, Italy.) and Burcharth (Burcharth, H.F., 1993. Structural integrity and hydraulic stability of Dolos armour layers. Series Paper 9, published by the Department of Civil Engineering, Aalborg University, Denmark, 1993.), who also presented design diagram for determination of breakage of Dolosse in trunk sections. The paper presentes an expansion of this work to include breakage of Dolosse in round-heads and Tetrapods in trunk sections.

* Corresponding author. Fax: +45-981-42555.
[1] Present address: Infram, P.O. Box 81, 3890 AB Zeewolde, The Netherlands.

PII: S0378-3839(00)00010-7

The paper presents a simple dimensional empirical formula instead of diagrams for the estimation of the number of broken Dolosse and Tetrapods in prototype situations, because probabilistic design of breakwaters requires failure mode formulae with the associated uncertainties.

Keywords: Breakage; Dolosse; Tetrapods

1. Introduction

Slender complex types of armour units like Tetrapods and Dolosse have limited strength when unreinforced. Assessment of risk of breakage is therefore just as important as the assessment of hydraulic stability. A previous systematic investigation of stresses in armour units resulted in design diagrams for Dolos armour in a trunk section exposed to head-on irregular waves (Burcharth, 1993).

The diagrams give the relationship between the central estimate of percentage of Dolosse which will break given the significant wave height, the Dolosse mass and waist ratio, and the tensile strength of the concrete. The diagrams are suitable for conventional deterministic design, but not directly applicable in a probabilistic design procedure as the uncertainty is not given. The probabilistic approach is to be preferred because it takes into account the various sources of uncertainties involved in the highly stochastic nature of wave–armour interaction. Probabilistic design of breakwaters is described in Burcharth (1992). This approach presumes that failure mode formulae signifying the various types of wave–structure interaction are given as well as the associated uncertainties. Such model uncertainty should be given by its probability distribution. A normal distribution defined by its mean value and standard deviation is often used as an approximation to unknown distributions.

The paper presents a design formula for the estimation of the number of armour units that will break in Dolos trunk sections and roundheads, and in Tetrapod trunk sections. The related formula uncertainties are given in the form of the coefficient of variation based on the assumption of a normal distribution. The formula is then directly applicable in probabilistic design procedures and reliability analysis of existing breakwaters.

The experimental and theoretical procedures for stress determination follow the method by Burcharth et al. (1991) and Burcharth (1993). Consequently, only a brief outline of the method is given in this paper. The stress determination is handled as a probabilistic problem due to the highly stochastic nature of wave loads, the complex shape of armour units and their random placement. Consequently, a very large number of situations should be investigated. This could be done at reasonable costs only by small scale experiments using a load cell technique in hydraulic model tests combined with calibration based on specific prototype experiments. The use of small scale experiments made it very important to analyze the stress scaling laws, cf. Section 3.

2. Loads on armour units and stress characteristics

The different types of mechanical loads on armour units and their origins are listed in Table 1.

Table 1
Types and origins of mechanical loads on armour units

TYPES OF LOADS		ORIGIN OF LOADS
Static		Weight of units Prestressing of units due to wedge effect and arching caused by movement under wave attacks
Dynamic	Pulsating	Gradually varying wave forces Earthquake
	Impact	Collisions between units when rocking or rolling, collision with underlayers or other structural parts Missiles of broken units Collisions during handling, transport and placing High-frequency wave slamming

The present study excludes the effect of earthquake, missiles of broken units, and collision during handling, transport and placing.

Related to the types of loading the stresses in the armour units are characterized as static, pulsating and impact stresses, cf. Fig. 1 which shows a typical stress time history.

3. Stress scaling laws for homogeneous armour units

Because the two main failure modes for concrete armour layers, namely displacements (hydraulic instability) and breakage (structural instability), are interrelated, they have to be studied together. However, in small Froude scale models as used for

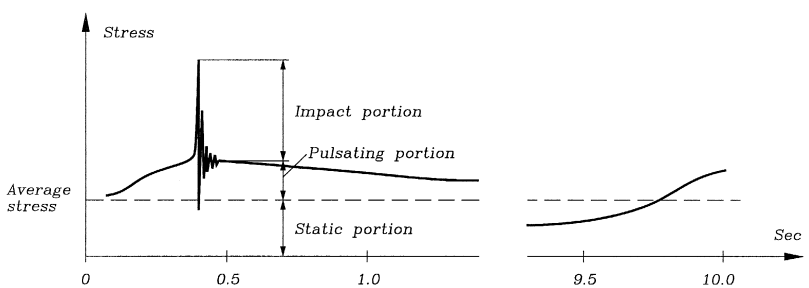

Fig. 1. Illustration of stress time history from a slender armour unit.

Table 2
Notation related to stress scaling laws

λ	Scale ratio, model value/prototype value
σ	stress, i.e. force per unit area
V	velocity
L	characteristic length
M	mass
F	force
ρ	mass density
g	gravitational acceleration
E	dynamic modulus of elasticity
C	$=\sqrt{\frac{E}{\rho}\frac{1-\mu}{(1+\mu)(1-2\mu)}}$ speed of stress wave (longitudinal wave in elastic medium)
μ	Poisson's ratio
Δ	$=(\rho_A/\rho_W)-1$
subindex	M for model
—	P — prototype
—	A — armour
—	W — water

displacement studies, the stress levels are too small to cause any breakage of model armour units when made of mortar or other conventional materials. Stresses recorded in small Froude scale models therefore have to be upscaled to prototype and compared with prototype concrete strength in order to identify possible breakage.

The stress scaling laws for systems with geometrical similarity and exposed to the same gravitational field are discussed in Burcharth (1993). A summary is given below. The used notation is given in Table 2. It should be noted that local crushing of the concrete in the impact zone is not dealt with as it has little importance related to armour stability for interlocking types of units. The scaling law for local crushing is quite different from the laws presented in this paper.

3.1. Static stresses

Static stresses are caused by gravitational effects.

3.1.1. Dry conditions

$$\lambda_{\sigma_{\text{Static}}} = \frac{F_M/L_M^2}{F_P/L_P^2} = \frac{M_M g_M/L_M^2}{M_P g_P/L_P^2} = \frac{\rho_{A,M} L_M^3 g_M/L_M^2}{\rho_{A,P} L_P^3 gP/L_P^2}$$
$$= \lambda_{\rho_A}\lambda_L\lambda_g \tag{1}$$

3.1.2. Submerged conditions

$$\lambda_{\sigma_{\text{Static}}} = \frac{(\rho_{A,M}-\rho_{W,M})L_M^3 g_M/L_M^2}{(\rho_{A,P}-\rho_{W,P})L_P^3 g_P/L_P^2} = \lambda_{\rho_W}\lambda_\Delta\lambda_L\lambda_g \tag{2}$$

Eq. (1) is excluded because the large stresses occur under submerged conditions. With $\lambda_g = 1$, Eq. (2) is simplified to $\lambda_{\sigma_{\text{Static}}} = \lambda_{\rho_w} \lambda_L$, because in the model tests $\rho_{W,M} = 1.00$ t/m^3 and $\rho_{A,M} = 2.29$ t/m^3 are chosen to obtain $\Delta = 1.29$ which corresponds to typical prototype conditions where $\rho_{W,P} = 1.025$ t/m^3 and $\rho_{A,P} = 2.3$–2.4 t/m^3.

3.2. Pulsating stresses

Pulsating stresses are caused by gradually varying wave forces (non-impulsive forces).

The wave forces might be expressed by the Morison equation

$$F = C_I \rho_W \dot{V}_W L^3 + C_D \frac{1}{2} \rho_w V_W^2 L^2 \tag{3}$$

The scaling law for the inertia term is

$$\lambda_{F_I} = \frac{C_{I,M} \rho_{W,M} \dot{V}_{W,M} L_M^3}{C_{I,P} \rho_{W,P} \dot{V}_{W,P} L_P^3} = \lambda_{C_I} \lambda_{\rho_w} \lambda_L^3 \tag{4}$$

because $\lambda_{\dot{V}} = 1$ in a Froude model.

The scaling law for the drag term is

$$\lambda_{F_D} = \frac{C_{D,M} \rho_{W,M} V_{W,M}^2 L_M^2}{C_{D,P} \rho_{W,P} V_{W,P}^2 L_P^2} = \lambda_{C_D} \lambda_{\rho_W} \lambda_L^3 \tag{5}$$

because $\lambda_V = \lambda_L^{0.5}$ in a Froude model.

Under the assumption that λ_{C_I} and λ_{C_D} are 1, which is correct for high Reynolds' numbers, i.e. larger than approximately 10^4 to 10^6, depending on the shape of the units, then Eqs. (4) and (5) merge into the same scaling law, and the scaling law for the related rigid body stresses reads

$$\lambda_{\sigma_{\text{Pulsating}}} = \lambda_{\rho_W} \lambda_L \tag{6}$$

3.3. Duration of impacts

When two solid bodies collide, the impact force and the related stresses will depend on the duration of the impact, i.e. the time of contact, τ. Due to the nonlinear material properties of concrete and to the complex shape of slender armour units, it is not possible to establish a formula by which τ can be quantified. However, it is sufficient for the present research to formulate a qualitative expression for τ. In the following are discussed two realistic models for estimation of τ. It is shown that for geometrically similar systems and constant Poisson's ratio it is reasonable to assume

$$\tau \sim L \sqrt{\frac{\rho_A}{E_A}} \quad \text{since} \quad C = \frac{L}{\tau} \sim \sqrt{\frac{E_A}{\rho_A}} \tag{7}$$

where C is the speed of the shock waves, and $\sim$ means proportional to.

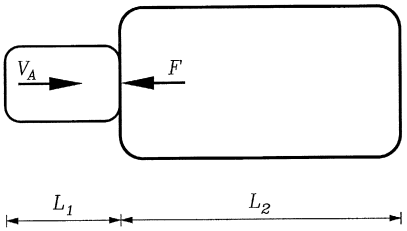

L_1 and L_2 are proportional to the characteristic length L of the system.

Fig. 2. Illustration of impact between blunt bodies.

3.3.1. Case 1. Impacting blunt bodies of identical linear elastic material

Fig. 2 illustrates impact between blunt bodies. It is assumed that the impact generates mainly one-dimensional compression longitudinal shock waves which travel with the rod wave speed, $C = \sqrt{E_A/\rho_A}$, the distances L_1 and L_2 to the free edges, where they are reflected as tension waves. The two bodies will lose contact at the first return of a tension wave to the impact surface. Consequently, because $L_1 < L_2$

$$\tau = \frac{2L_1}{C} = \frac{2L_1}{\sqrt{\frac{E_A}{\rho_A}}} \quad \text{or} \quad \tau \sim L\sqrt{\frac{\rho_A}{E_A}}$$

3.3.2. Case 2. Slender body impacted by blunt body of identical linear elastic material

The impacting blunt body of mass M_A hits the slender structure of mass $M \sim M_A$ with impact velocity V_A by which a vibration mainly caused by bending and shear is initiated, cf. Fig. 3. It is assumed that the maximum value of τ corresponds to contact

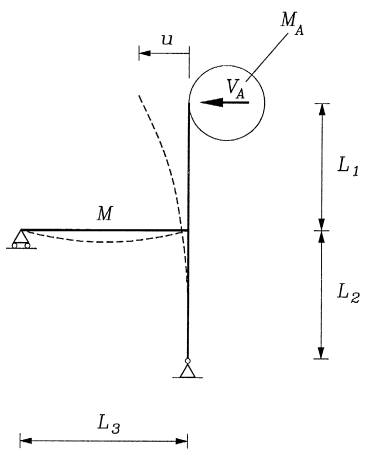

$\sim$: proportional to

$L_1 \sim L_2 \sim L_3 \sim L$

$M \sim M_A \sim \rho_A L^3$

Fig. 3. Illustration of slender body impacted by blunt body.

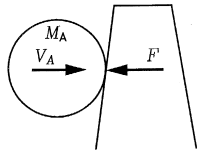

$$V_A \sim \sqrt{2gL}$$
$$M_A \sim \rho_A L^3$$

Fig. 4. Illustration of free-fall impinging body.

between the two bodies during approximately one half period T of the first mode of vibration for the slender body.

If it is assumed that the slender structure has a linear response corresponding to transverse impacts on free and simply supported beams, then the system corresponds in principle to a mass–spring system with spring stiffness

$$k \sim \frac{E_A I}{L^3} \tag{8}$$

where $I \sim L^4$ is the moment of inertia.

The deflection time defined as one half period of the first mode of vibration is

$$\tau \simeq \frac{T}{2} \simeq \sqrt{\frac{M_A + M_o}{k}} \tag{9}$$

where $M_o \sim M \sim M_A \sim \rho_A L^3$ is the modal mass of the slender body.

From Eqs. (8) and (9) is then obtained Eq. (7). This conclusion was already presented in Burcharth (1981).

3.4. Impact stresses

Impact stresses are caused by collision of two solid bodies or by water impinging (slamming) on a solid body.

3.4.1. Case 1. Scale law in case of free fall impinging body

In case of free fall impinging body, cf. Fig. 4, the momentum equation reads

$$F\tau = M_A \Delta V_A \sim M_A V_A \tag{10}$$

where τ is the duration of the impact and ΔV is the velocity difference of the impinging body before and after the collision. $\Delta V \sim V_A$ is due to the assumed constant coefficient of restitution.

Inserting Eq. (7) in Eq. (10) yields

$$F \sim \frac{\rho_A L^3 (gL)^{0.5} E_A^{0.5}}{L \rho_A^{0.5}} = \rho_A^{0.5} E_A^{0.5} g^{0.5} L^{2.5}$$

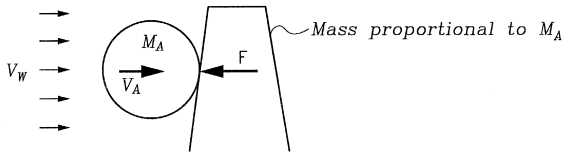

Fig. 5. Illustration of impinging body driven by flow.

Using $\sigma = F/L^2$ and introducing $\lambda = (\text{model value})/(\text{prototype value})$, we obtain

$$\lambda_{\sigma_{\text{Impact}}} = \left(\lambda_{\rho_A}\lambda_{E_A}\lambda_L\lambda_g\right)^{0.5} \tag{11}$$

3.4.2. Case 2. Scale law of impinging body affected only by flow forces

In case the impinging body is driven by flow, cf. Fig. 5, V_A is found from Newton's 2nd law

$$F_W = M_A\frac{\mathrm{d}V_A}{\mathrm{d}t} \tag{12}$$

$$V_A = \frac{F_W}{M_A}t = \frac{F_W}{\rho_A L^3}t \tag{13}$$

where F_W is the flow force on the impinging body.

By the use of Eqs. (7), (10) and (13) is obtained

$$F \sim \frac{\rho_A L^3 F_W\, tE_A^{0.5}}{\rho_A L^3 L\rho_A^{0.5}} = \rho_A^{-0.5}L^{-1}F_W\, tE_A^{0.5}$$

$$\lambda_{\sigma_{\text{Impact}}} = \lambda_{\rho_A}^{-0.5}\lambda_L^{-3}\lambda_{F_W}\lambda_t\lambda_{E_A}^{0.5} \tag{14}$$

Because in the Froude model, $\lambda_{F_W} = \lambda_{\rho_W}\lambda_L^3$ and $\lambda_t = \lambda_L^{0.5}$, then

$$\lambda_{\sigma_{\text{Impact}}} = \lambda_{\rho_A}^{-0.5}\lambda_{\rho_W}\lambda_{E_A}^{0.5}\lambda_L^{0.5} \tag{15}$$

The variation in F_W due to viscous effects is neglected. This, however, introduces some unknown bias, the size of which depends on the Reynolds number range.

3.4.3. Case 3. Collision between impinging water (slamming) and a solid body

The air-cushioning effect is neglected because it is unlikely that air-pockets will be entrapped due to the limited size and rounded shape of the elements. As characteristic velocity of the water, V_W, is taken, the wave celerity of depth limited waves, $V_W \sim \sqrt{gL}$, cf. Fig. 6.

τ is assumed given by Eq. (7) because the solid body stress wave is reflected from a free surface of the armour unit long time before reflection from a free surface of the wave (travel distance $\backsimeq H_s >$ dimension of armour unit; shock wave speed is smaller in water than in concrete) and the deflection time will be shorter than the transverse time of the elastic wave in the water.

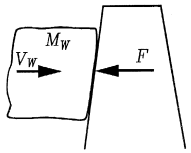

$$V_W \sim \sqrt{g\,L}$$
$$M_W \sim \rho_W\,L^3$$

Fig. 6. Illustration of collision between impinging water and a solid body.

From the momentum equation

$$F\tau = M_W \Delta V_W \sim M_W V_W \tag{16}$$

and Eqs. (7) and (13) is obtained

$$F \sim \frac{\rho_W L^3 g^{0.5} L^{0.5} E_A^{0.5}}{L \rho_A^{0.5}} = \rho_A^{-0.5} \rho_W E_A^{0.5} L^{2.5} g^{0.5}$$

and consequently

$$\lambda_{\sigma_{\text{Impact}}} = \lambda_{\rho_A}^{-0.5} \lambda_{\rho_W} \lambda_{E_A}^{0.5} \lambda_L^{0.5} \lambda_g^{0.5} \tag{17}$$

The difference between the above three scaling laws (Eqs. (11), (15) and (17) is related to the scales of the densities only, because generally

$$\lambda_{\rho_A} \neq \lambda_{\rho_A}^{-0.5} \lambda_{\rho_W} \tag{18}$$

As long as the model is made of approximately the same concrete as the prototype, Eq. (11) can be chosen as the scaling law for the impact stresses, as it introduces less than 1% error for $0.97 \leq \lambda_{\rho_A} \leq 1.00$ and $0.98 \leq \lambda_{\rho_W} \leq 1.00$.

4. Failure criterion

The tensile strength of unreinforced concrete is an order of magnitude smaller than the compressive strength. Concrete is thus a brittle material. In slender units, failures start almost exclusively with cracking where the tensile stress exceeds the concrete tensile strength. The most critical spots are: for Dolosse at the surface of the shank cross-section close to the fluke; for Tetrapods at the surface of the cross-sections close to the root of the legs.

The failure criterion is taken as

$$\sigma_T \geq S \quad \text{failure} \tag{19}$$
$$\sigma_T < S \quad \text{no failure}$$

where σ_T is the *maximum principal tensile* stress occurring in the armour units, and S is the concrete tensile strength. It should be noted that Eq. (19) also defines failure when only a small surface crack appears and the cross-section still has considerable bearing capacity. σ_T can be calculated from the cross-sectional component forces and moments, see Burcharth et al. (1991) where σ_T is given as function of bending moment, torque, shear and axial force for circular and octagonal sections.

5. Load-cell and apparent elasticity

In order to record component forces in a cross-section from which the maximum principal tensile stress σ_T can be calculated, ultra sensitive strain gauge load cells were mounted inside 200 g Dolosse and 290 g Tetrapods as shown in Fig. 7. Load cell instrumentation of armour units was first applied by Delft Hydraulics Laboratory (DHL, 1980) and Scott et al. (1986). The applied load cell is a further development by Coastal Engineering Research Center (CERC), U.S. Army Corps of Engineers, Vicksburg (Markle, 1990) as part of a Dolos research cooperation with Aalborg University. This again was initiated on the basis of the CERC Crescent City Prototype Dolosse Study (Howell, 1985, 1988) and on full scale testing of Dolosse by Aalborg University (Burcharth, 1981).

The load cell is positioned in the most critical section of the armour units. Only bending moments and torque are recorded by the load cell, leaving stress contributions from axial and shear forces out. This is acceptable as it was found from the ramp tests in the dry with fully instrumented 200 kg Dolosse (Burcharth et al., 1991) that negligence of axial and shear forces most likely results in overestimation of σ_T for larger stress levels. Thus, the negligence is on the safe side.

The scaling law for impact stresses in the armour units is related to the elasticity E_A of the material, cf. Eq. (11). Unfortunately, the insertion of the load-cell destroys the homogeneity of the material, which again changes the dynamic response. Consequently, Eq. (11) cannot be applied. However, by comparing very well defined small scale results for the load-cell instrumented units with results of similar large scale impact tests with homogeneous large and full scale units, it was possible to define an *apparent modulus of elasticity*, E, to be substituted for E_A in Eq. (11).

The drop and pendulum test results of 1.5–30 tons Dolosse by Burcharth (1981), and the transverse pendulum test results of 1.4 tons Dolosse by Lin et al. (1986) have been

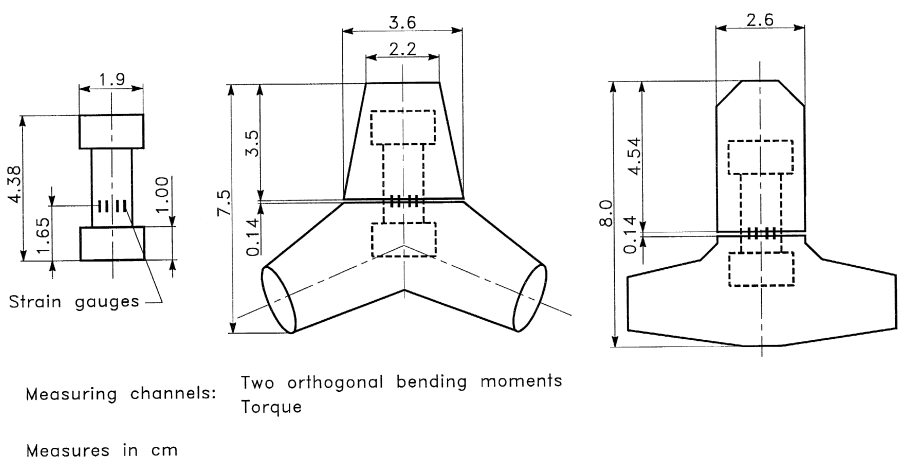

Fig. 7. 187 g Dolos and 290 g Tetrapod with strain gauge mounted load-cells.

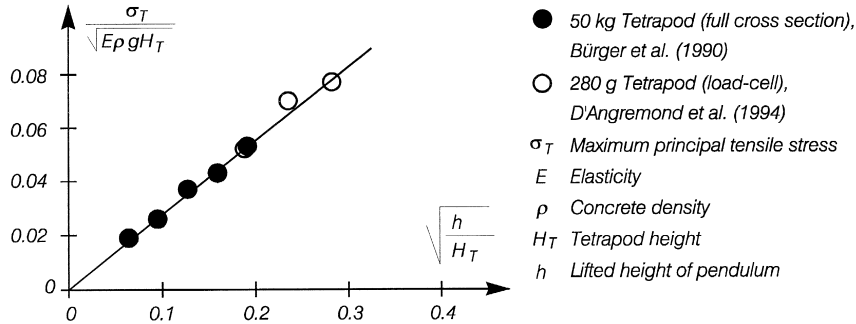

Fig. 8. Comparison of pendulum test results of the large scale Tetrapod with surface mounted strain gauges and the small scale Tetrapod with load-cell. Apparent modulus of elasticity $E = 4800$ MPa.

used for comparison with the results of the model Dolosse with load-cell, while the pendulum test results of 50 kg Tetrapods by Bürger et al. (1990) have been used for the model Tetrapods with load-cell. The impact calibration results of the model Dolosse with load-cell resulting in an average apparent modulus of elasticity of $E = 3500$ MPa have been published in Burcharth (1993). The result of impact calibration of the model Tetrapods was $E = 4800$ MPa as shown in Fig. 8. For the applied pendulum test set-up, reference is made to Bürger et al. (1990).

A way of checking the apparent elasticity is to compare the impact duration of the small load-cell mounted units with those of the various large size units performed by Terao et al. (1985), by Howell, and by Melby and Turk (1994), cf. Eq. (7). Fig. 9 shows the ratio of dimensionless stress of various sizes of Dolosse using the apparent elasticity of the 200 g Dolos. Even though there is a large scatter, it can be seen that most ratios

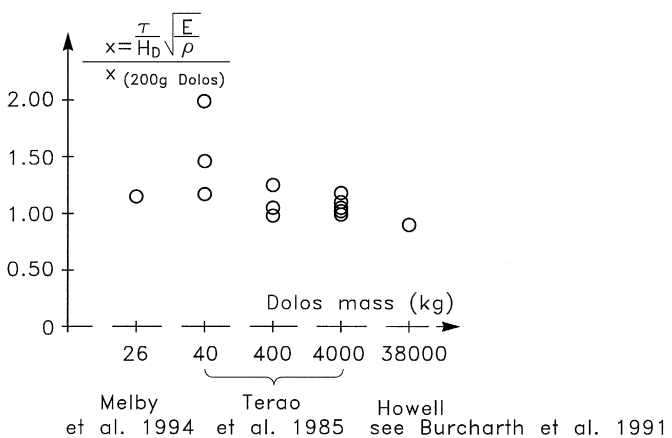

Fig. 9. Ratios of the dimensionless impact duration of large scale Dolosse against 200 g Dolos with load-cell (drop and pendulum tests). Apparent modulus of elasticity $E = 3500$ MPa.

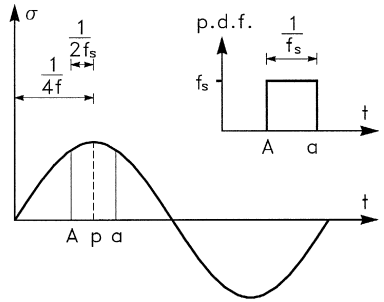

$$\sigma = \sigma_p \sin(2\pi f t)$$

Fig. 10. Sinusoidal stress signal.

are around the value of 1, thus confirming the value of the apparent elasticity. The single high value of Terao et al. for a 40-kg Dolos is not explained by the researchers.

6. Sampling frequency

The ultra short duration of solid body impact loads and wave slamming requires a very high sampling frequency in order to obtain a reliable estimate of the stress peak. The following analysis gives the underestimation of the stress peak corresponding to a certain sampling frequency.

Suppose the stress signal is recorded at frequency f_s and the stress signal is sinusoidal with the maximum stress σ_p and frequency f, cf. Fig. 10.

The most unfavorable case is when the two adjacent sampling points, A and a, are symmetrically located around the center of the peak p. For this case the sampled maximum stress σ_A is

$$\sigma_A = \sigma_p \sin(2\pi f t_A) = \sigma_p \sin\left(2\pi f\left(\frac{1}{4f} - \frac{1}{2f_s}\right)\right) \tag{20}$$

and *the maximum relative error* is

$$\frac{\sigma_p - \sigma_A}{\sigma_p} = 1 - \sin\left(\pi\left(\frac{1}{2} - \frac{f}{f_s}\right)\right) \tag{21}$$

On the other hand, the sampling points will be uniformly distributed along the length $(A - a)$, the average of the sampled maximum stress is

$$\begin{aligned}\overline{\sigma} &= \int_{t_A}^{t_a} \sigma_p \sin(2\pi f t)\, f_s \mathrm{d}t \\ &= \frac{\sigma_p}{2\pi}\frac{f_s}{f}\left(\cos\pi\left(\frac{1}{2} - \frac{f}{f_s}\right) - \cos\pi\left(\frac{1}{2} + \frac{f}{f_s}\right)\right)\end{aligned} \tag{22}$$

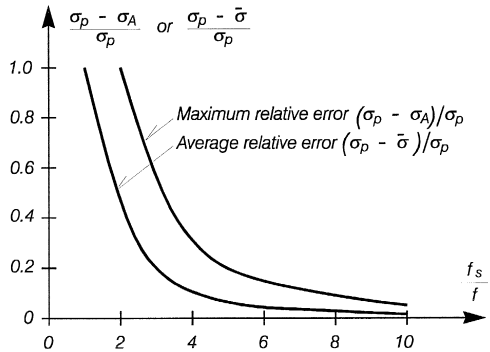

Fig. 11. Maximum relative error and average relative error due to limited sample frequency (sinusoidal stress signal).

and *the average relative error* is

$$\frac{\sigma_p - \bar{\sigma}}{\sigma_p} = 1 - \frac{1}{2\pi}\frac{f_s}{f}\left(\cos\pi\left(\frac{1}{2} - \frac{f}{f_s}\right) - \cos\pi\left(\frac{1}{2} + \frac{f}{f_s}\right)\right) \tag{23}$$

The maximum relative error and the average relative error are depicted in Fig. 11.

However, the actual impact signals are not sinusoidal, cf. Fig. 12. In order to check the influence of the sampling frequency, a series of Dolos pendulum tests with different sampling frequencies have been performed. The results are depicted in Fig. 12. It can be seen that the sinusoidal results hold also for the actual impact signal when the signal sampled with $f_s = 10\,000$ Hz is considered to be the real one.

In the Dolos hydraulic model test, the applied sampling frequency is $f_s = 6000$ Hz and the damped natural frequency of the instrumented Dolosse $f = 1500$ Hz, i.e. $f_s/f = 4$. From Fig. 11 it is found that on average the sampled maximum impact stress is underestimated by 10% due to the limited sampling frequency. Therefore, in the data processing all sampled maximum impact stresses were increased by 10%.

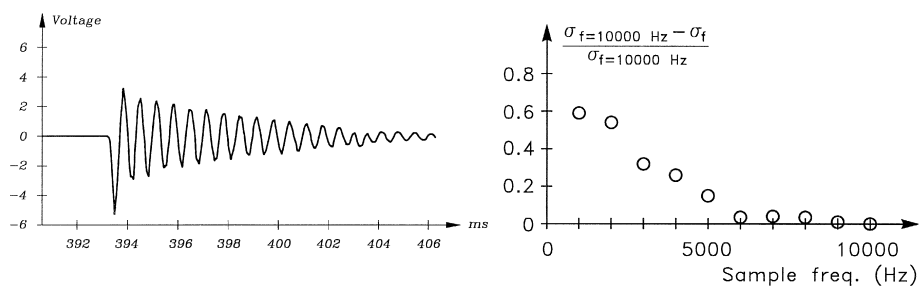

Fig. 12. Example of the impact signals of the 200 g load-cell instrumented concrete Dolosse ($f = 1500$ Hz) and the relative error of the Dolos pendulum test results as function of the sampling frequency.

7. Check on the dynamic amplification by wave slamming

It is well-known that resonance occurs when the frequency of the load is close to the natural frequency of the system. The instrumented model units have a lower elasticity, and hence a lower natural frequency, cf. Eq. (7). In order to check if the reduced natural frequency of the Dolosse is close to the wave slamming frequency, and hence introduces dynamic amplification, the frequency of the wave slamming on the Dolos armour layer was recorded by a pressure transducer installed in the stem of the Dolos. The pressure transducer did in all tests face breaking waves. The results are given in Fig. 13, showing the highest frequency of the wave slamming on the Dolos armour to be 330 Hz, far away from the natural frequency of 1500 Hz for the Dolosse with the load-cells. Consequently, no dynamic amplification are present in the model tests.

8. Brief description of experiments

The models used in the experiments had a front slope of 1:1.5 and were armoured with conventional double layers of Dolosse or Tetrapods. Generally, the slopes were non-overtopped during the tests. A detailed description of the model tests, which included the trunk of the Dolos breakwater, the round-head of the Dolos breakwater and the trunk of the Tetrapod breakwater, has been given in Burcharth and Liu (1992), Burcharth et al. (1995) and d'Angremond et al. (1994), respectively. Table 3 gives an outline of the test conditions.

In the tests with the trunk of Dolos breakwaters, three types of dolos waist-to-height ratios were applied, namely 0.325, 0.37 and 0.42, while in the round-head tests, only the waist-to-height ratio of 0.37 was applied.

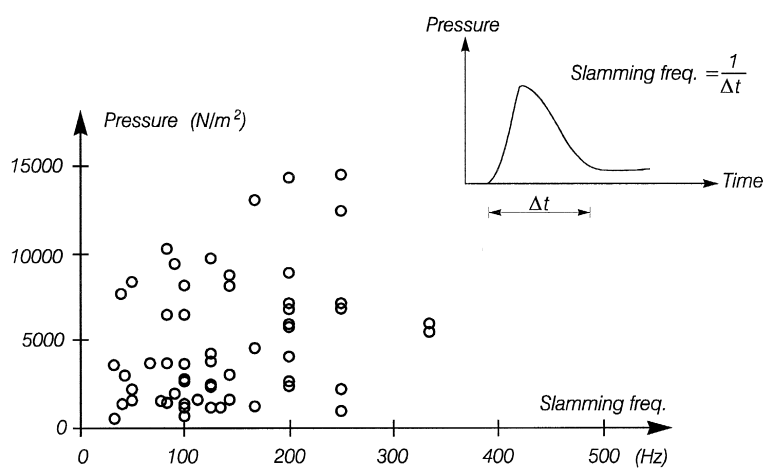

Fig. 13. Recorded frequencies of the wave slamming on 200 g pressure-cell instrumented Dolos armour units.

Table 3
Summary of the hydraulic model test conditions

	Dolos trunk	Dolos round-head	Tetrapod trunk
Breakwater slope α	1.5	1.5	1.5
Foreshore	1:20	horizontal	1:50
Water depth at toe (cm)	23	50	30 and 50
Height of breakwater (cm)	60	70	55 and 75
Mass of units (kg)	0.187	0.187	0.290
Concrete density (ton/m^2)	2.3	2.3	2.3
Packing density	0.74	0.74	1
Spectral peak period T_p (s)	1.5–3	1.5–2.5	1.3–2.8
Significant wave height H_s (cm)	5.7–17.7	5–13	8.8–27.3
Surf similarity parameter $\xi = (H_s/L_p)^{-0.5}$ tan α	3–7.5	3.8–7.5	2.7–4.1

Only head-on waves are applied in the round-head tests.

9. Distribution of stresses over the slope

The distribution of maximum principal tensile stress σ_T over the slope is of interest in order to identify the potential areas for armour breakage.

Fig. 14 shows typical distributions given by the 2% exceedence values of σ_T for each of the six instrumented Dolos positions for 10 and 50 ton Dolos of waist ratios 0.325 and 0.42 exposed to wave action levels, hydraulic stability number $N_S = (H_s)/(\Delta D_n) = 0.9$, 1.8 and 2.6. H_s is the significant wave height at toe and D_n the equivalent cubic length of the Dolosse.

The following conclusions can be drawn from the analyses of a large number of distributions of maximum σ_T in Dolosse over the slope:

- The contribution of the impact stress to the maximum principal tensile stress σ_T is generally less than 10% for $N_S \leq 2.0$.
- The impact stresses are relatively very small in the bottom layer, while the impact stresses are relatively very significant in the top layer.
- Breakage will in most cases start in the top layer in the zone just below SWL. This zone is more vulnerable to breakage than the zone above SWL.

10. Development of breakage formulae

10.1. Stress time series in prototype scale

Time series of the maximum principal tensile stress, σ_T, in a critical cross-section of the load-cell instrumented units, is calculated from the load cell strain recordings.

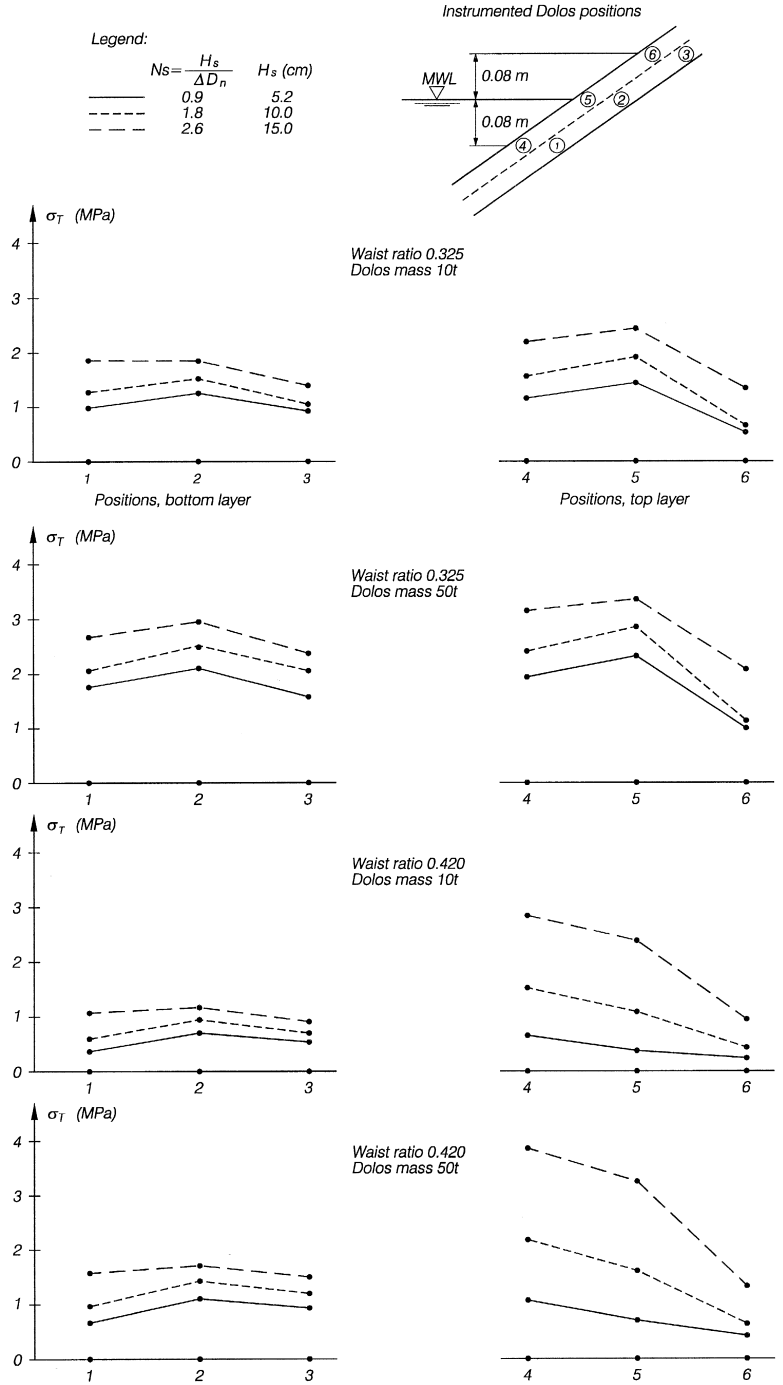

Fig. 14. Distribution of σ_T over the slope. 2% stress exceedence probability level. The armour layer is formed of two layers of randomly placed Dolosse.

Due to the involved two different scaling laws for non-impact and impact stresses, Eqs. (6) and (11), it is necessary to separate the stress signal into an impact portion and a non-impact portion, the latter covering static plus pulsating stresses. Fig. 15 illustrates how the model scale stress, $\sigma_{T,M}$, is separated.

The transformation of the stress time series from model to prototype is given by

$$\sigma_{T,P} = \lambda_L^{-1}\sigma_{\text{non-impact},M} + (\lambda_L\lambda_E)^{-0.5}\sigma_{\text{impact},M}/1.4 \quad (24)$$

where the impact stress is divided by 1.4 in order to account for the fact that the concrete dynamic strength is approx. 1.4 times the static strength (Burcharth, 1984), so that $\sigma_{T,P}$ can be directly compared with the concrete static strength.

10.2. Conversion of relative breakage from model to prototype scale

The following example explains the determination of the relative breakage of Dolosse at prototype scale.

In the hydraulic model tests are used six instrumented Dolosse with the waist ratio $r = 0.32$, and three test runs with $H_s = 11.2$ cm are performed, thus giving a total of 18 stress time series.

1. Assume that the mass of the prototype Dolosse is 10 tons, corresponding to the length scale $\lambda = 37$. The wave height in the prototype is then 4.2 m.
2. By the use of Eq. (24) the 18 model stress time series are converted into 18 prototype stress time series.
3. The maximum stress in each prototype stress time series is identified, thus giving 18 maximum stress values.
4. If it is assumed that the concrete strength is 3 MPa, and there is one of the 18 maximum stresses which are bigger than 3 MPa, then the relative breakage of the prototype units is $B = 1/18 = 0.056$

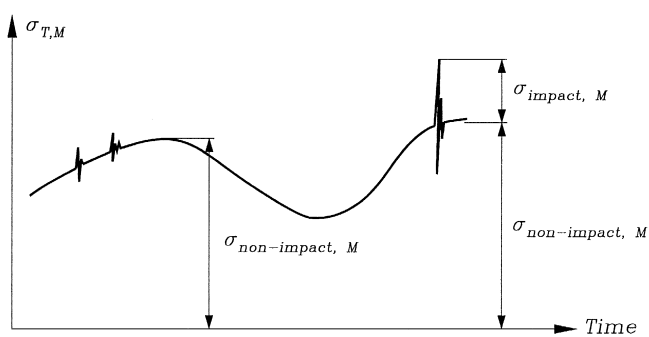

Fig. 15. Separation of σ_T in the stress time series.

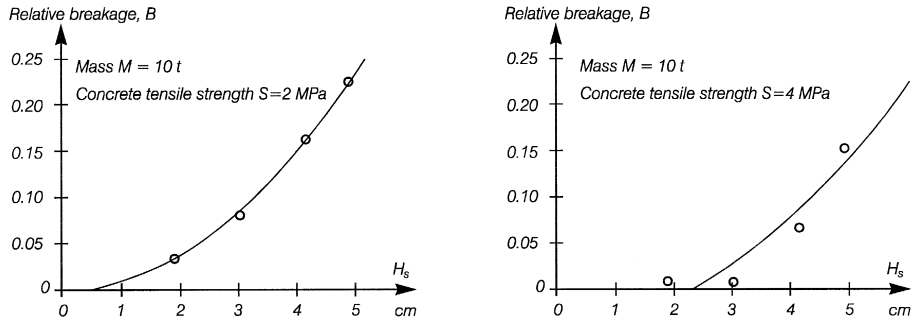

Fig. 16. Examples of relative breakage vs. wave height (round-head of Dolos breakwater).

By applying the same procedure to the tests with other significant wave heights, we obtain the following relationship between the relative breakage B and the significant wave height H_s

$$B = A_0 H_s^2 + A_1 \tag{25}$$

where A_0 and A_1 are fitted parameters, the values of which depend on the mass of the prototype units and the concrete strength, cf. the examples given in Fig. 16. A_0 is dimensional and A_1 non-dimensional.

With respect to the role of static stress, it was found that the static stress on its own will hardly cause any breakage of Dolosse and Tetrapods under 50 tons. On the other hand it has been shown that for the large units the static stress often occupies large proportions of the strength, which means that there is little residual strength to resist pulsating and impact stresses. Thus, it is important that large units are not exposed to severe rocking or displacement.

10.3. Breakage formula

For practical engineering, Eq. (25) is not convenient. This is because values of A_0 and A_1 must be found for each prototype unit size and concrete strength. It is desirable to present the results in a formula containing also armour unit size and concrete tensile strength.

The main parameters which determine the armour unit breakage are the unit mass M, the concrete properties (density ρ_a, modulus of elasticity E and tensile strength S), the sea state (water depth d, significant wave height H_s and peak wave period T_p) and the breakwater geometry parameters (slope, armour unit placement and packing density).

In the hydraulic model tests, a certain breakwater geometry has been applied, cf. the description of the experiment. Within the tested range of parameters there seems not to be a significant influence of water depth and wave period on the breakage. The parameters to be considered are thus limited to M, ρ_a, E, $S$and H_s.

Because of the different scaling laws for the non-impact and impact stresses, various nondimensional forms of a breakage formula produce poor fitting to the test data. Instead it was decided to present a simple dimensional formula, covering the usual design situations. The formula for relative breakage takes the form

$$B = C_0 M^{C_1} S^{C_2} H_s^{C_3} \tag{26}$$

Table 4
Fitted parameters for the breakage formula, Eq. (26), and valid parameter ranges
Valid for: non-overtopped, slope 1:1.5, Dolos packing density 0.74, Tetrapod packing density 1.0. Mass of armour unit in tons $2.5 \leq M \leq 50$. Concrete tensile strength in MPa $2 \leq S \leq 4$. Relative number of displaced armour units $D \leq 10\%$.

	Waist ratio	Variational coefficient of C_0	C_0	C_1	C_2	C_3
Trunk of Dolosse	0.325	0.188	0.00973	−0.749	−2.58	4.143
	0.37	0.200	0.00546	−0.782	−1.22	3.147
	0.42	0.176	0.01306	−0.507	−1.74	2.871
Round-head of Dolosse	0.37	0.075	0.025	−0.65	−0.66	2.42
Trunk of Tetrapods		0.25	0.00393	−0.79	−2.73	3.84

where

B	Relative breakage
M	Armour unit mass in ton
S	Concrete tensile strength in MPa
H_s	Significant wave height in meter
C_0, C_1, C_2, C_3	Fitted parameters

The mass density, ρ_A, and the modules of elasticity, E, of the concrete material are assumed to be 2.3 tons/m^3 and 30 000 MPa, respectively.

The data base for the formula fitting is produced as follows:

Prototype unit masses, M, from 2.5 to 50 tons with increment of 2.5 tons are applied. Concrete tensile strengths, S, from 2 to 4 MPa with increment of 0.5 MPa are applied. For each given $M$and S, the values of A_0 and A_1 in Eq. (25) are obtained as described before. Then the relative displacement of the unit is assumed to be 1%, 2%, …, 10%. The corresponding significant wave height is calculated by the hydraulic stability formulae given by Burcharth (1993) and van der Meer (1988) for Dolosse and Tetrapods, respectively. The relative breakage is calculated by Eq. (25).

The least square method of multi parameter linear fitting is applied to fit the obtained data sets to Eq. (26). The fitted parameters are listed in Table 4. Examples of the fitting are shown in Fig. 17. The two examples illustrates the minimum and the maximum scatter for trunk sections, cf. the coefficient of variation given in Table 4. The uncertainty inherent in each data point is not included in the calculations of the coefficient of variation. Although there is significant scatter the formula can predict the order of magnitude of the breakage sufficiently accurate for design purpose seen on the background of the many other sources of uncertainty related to design.

11. Verification of the formula

The breakage formula have been checked against observed behaviour of prototype Dolos breakwaters and reasonable agreement was found, cf. Table 5. The formula does

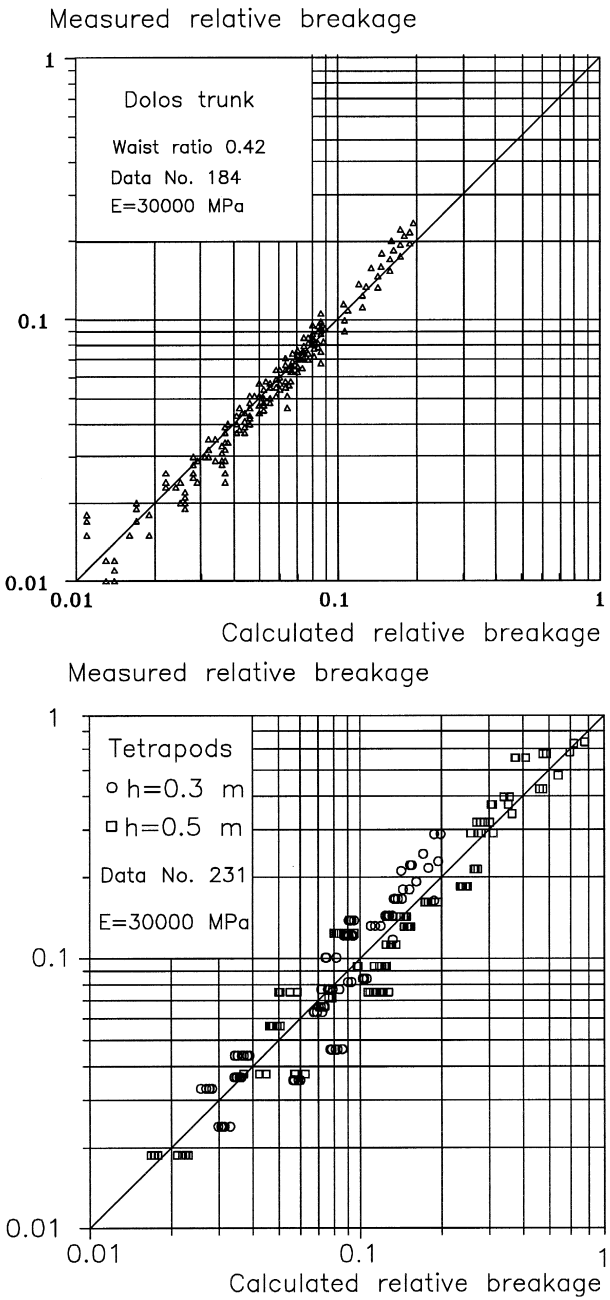

Fig. 17. Fitting of the breakage formula. *h* is the water depth at the toe.

Table 5
Observed and predicted damage of some Dolos breakwaters

	Crescent City, USA	Richards Bay	Sines POR
H_s (m)	10.7[a]	5[b]	9[c]
Slope	1:4	1:2	1:1.5
Dolos mass (ton)	38	20	42
Waist ratio	0.32	0.33	0.35
Dolos packing density	0.85	1	0.83
Concrete density (kg/m^3)	2500	2350	2400
Elasticity (MPa)[d]	30,000	30,000	30,000
Tensile strength (MPa)[d]	3	3	3
Reported displacement	7.3%		
Reported breakage	19.7%		
Reported displacement + breakage[e]	26.8%	4%	collapse
Predicted displacement	3.6%	0.6%	3.6 %
Predicted breakage by the diagrams[f]	$>10\%$	5%	$>10\%$
Predicted breakage by the formula	68%	4.8%	31%

[a] Depth limited in front of breakwater.
[b] In front of breakwater.
[c] Offshore $\approx$ in front of breakwater.
[d] Estimated values.
[e] Broken and displaced unit is counted only once.
[f] Design diagramme for Dolos breakage is given in Burcharth (1993).

not predict much better results than the Dolosse design diagrams by Burcharth (1993). This could not be expected as the same data sets are used.

A better verification of the formula is certainly wanted, but it has been very difficult to find Dolos breakwaters where the breakage has been carefully monitored. Also, breakage could be due to less careful placement during construction and poor concrete quality. The formula for Tetrapods breakage has not been verified by comparison with prototype data.

12. Example of application

12.1. Dolos breakage: trunk vs. round-head

Table 6 gives the relative breakage of Dolosse in the trunk and the round-head of a breakwater in two situations where the significant wave height, the Dolos mass and the

Table 6
Example of Dolos breakage in trunk and round-head, determined by Eq. (26)

Input	Significant wave height H_s (m)	5	8
	Dolos mass M (tons)	10	20
	Concrete tensile strength S (MPa)	3	4
Result	Relative breakage, trunk (%)	2	3
	Relative breakage, round-head (%)	13	22

Table 7
Comparison between Dolosse and Tetrapods (breakwater trunk)

Input	Significant wave height $H_s = 8$ m Mass of Dolosse and Tetrapods $M = 20$ tons Concrete tensile strength $S = 3$ MPa			
	Dolosse			Tetrapods
Waist ratio	0.325	0.37	0.42	
Relative displacement (%)	3.6	5.6	10	5
Relative breakage (%)	17.8	6.0	10.6	5
Σ	21.4	11.6	20.6	10

concrete tensile strength are given. It shows that Dolosse in a round-head is much more vulnerable to breakage than the Dolosse in a trunk.

12.2. Breakage: Dolosse vs. Tetrapods

Table 7 gives the comparison of the relative displacement and the relative breakage of Dolosse and Tetrapods in a breakwater trunk. The relative displacement of Dolosse and Tetrapods is calculated according to Burcharth (1993) and van der Meer (1988), respectively. It can be seen that Tetrapods have almost the same hydraulic stability and structural integrity as Dolosse with waist ratio 0.37. The table indicates also that the optimal Dolos waist ratio is around 0.37, taking into consideration both the hydraulic stability (displacements) and structural integrity.

13. Conclusions

The paper first discusses the scaling laws for stresses in armour units. It is shown that static and pulsating stresses scale linearly with the length scale, whereas the impact stresses scale with the square root of the length scale. This means that the two categories of stresses must be separated in the model in order to produce a correct up-scaling of the total stresses in prototype situations.

The analysis of a large number of distributions of maximum principal tensile stresses in Dolosse over the slope reveals:

- The contribution of the impact stress to the maximum principal tensile stress σ_T is generally less than 10% for $N_S \leq 2.0$.
- The impact stresses are relatively very small in the bottom layer, while the impact stresses are relatively very significant in the top layer.
- Breakage will in most cases start in the top layer in the zone just below SWL. This zone is more vulnerable to breakage than the zone above SWL.

A simple dimensional empirical formula has been presented for the estimation of the number of broken Dolosse and Tetrapods in prototype situation, based on model tests

performed at Aalborg University and Delft Hydraulics. Within the tested range of parameters, there seems not to be a significant influence of water depth and wave period on the breakage. The formula contains only three variables, namely the unit mass, M, the concrete tensile strength, S, and the design significant wave height, H_s, cf. Eq. (26).

The formula shows that Dolosse in a round-head is much more vulnerable to breakage than Dolosse in a trunk. With respect to Dolos waist ratio, the formula indicates that the optimal Dolos waist ratio is around 0.37, taking into consideration both the hydraulic stability (displacements) and structural integrity.

The formula have been checked against observed behaviour of prototype Dolos armours and a reasonable agreement was found. However, the formula is not verified by comparison with the performance of prototype Tetrapod armour.

Acknowledgements

The research was funded jointly by the Danish Technical Research Council (STVF) under the programme *Marin Technique*and by the Commission of the European Communities, Directorate General for Science, Research and Development under MAST-contract MAS2-CT92-0042 *Rubble Mound Breakwater Failure Modes*. Mr. C.P. van Nes at Delft University of Technology, Mr. M.S. Jensen and Mr. J.B. Jensen at Aalborg University are acknowledged for their engagement in the experiment and data processing.

References

d'Angremond, K., van der Meer, J.W., van Nes, P., 1994. Stresses in Tetrapod armour units induced by wave action. In: Proceedings of the 24th International Conference on Coastal Engineering, Kobe, Japan.

Burcharth, H.F., 1981. Full-scale dynamic testing of Dolosse to destruction. Coastal Engineering 4.

Burcharth, H.F., 1984. Fatigue in breakwater armour units. In: Proceedings of the 19th International Conference on Coastal Engineering, Houston, TX, Sept. 1984.

Burcharth, H.F., 1992. In: Reliability Evaluation of a Structure at Sea. Proc. of the Short Course on Design and Reliability of Coastal Structures, Venice, Italy. pp. 597–644, Attached to the 23rd International Conference on Coastal Engineering.

Burcharth, H.F., 1993. Structural integrity and hydraulic stability of Dolos armour layers. Series Paper 9, published by the Department of Civil Engineering, Aalborg University, Denmark.

Burcharth, H.F., Howell, G.L., Liu, Z., 1991. On the determination of concrete armour unit stresses including specific results related to Dolosse. Coastal Engineering 15, 107–165.

Burcharth, H.F., Liu, Z., 1992. Design of Dolos armour units. In: Proceedings of the 23rd International Conference on Coastal Engineering, Venice, Italy.

Burcharth, H.F., Jensen, M.S., Liu, Z., d'Angremond, K., van der Meer, J.W., 1995. Design formula for breakage of Tetrapods. In: Draft presented at the Final Workshop of Rubble Mound Breakwater Failure Modes, Sorrento, Italy, November 1995.

Bürger, W.W., Oumeraci, H., Partenscky, H.W., 1990. Impact strain investigations on tetrapods results of dry and hydraulic tests, ASCE Proc. Seminar Stresses in Concrete Armor Units.

Howell, G.L., 1985. In: Proc. of Workshop on Measurement and Analysis of Structural Response in Concrete Armour Units, January 23–24. Waterways Experiment Station, Coastal Engineering Research Center, Vicksburg, MS, USA.

Howell, G.L., 1988. Measurement of forces on dolos armour units at prototype scale. In: Proc. 21st Int. Conf. on Coastal Engineering.

Lin, W.M., Rau, C., Su, R.L., 1986. The structural response of Dolos armour units under dynamic loading. In: Proc. 20th Int. Conf. Coastal Engineering, Taipei, Taiwan.

Markle, D.G., 1990. Crescent City instrumented model dolos study. In: ASCE Proc. Seminar Stresses in Concrete Armor Units.

Melby, J.A., Turk, G.F., 1994. Scale and modeling effects in concrete armor experiments. In: Coastal Dynamics'94, Barcelona, Spain.

Scott, R.D., Turcke, D.J., Baird, W.F., 1986. A unique instrumentation scheme for measuring loads in model Dolos units. In: Proc. 20th Int. Conf. Coastal Engineering.

Terao, T., Terauchi, K., Ushida, S., Shiraishi, N., Kobayashi, K., Gahara, H., 1985. Prototype testing of Dolosse to destruction. In: Proc. Workshop on Measurement and Analysis of Structural Response in Concrete Armor Units. U.S. Army Corps of Engineers, CERC, WES, Vicksburg, MS, USA.

van der Meer, J.W., 1988. Stability of cubes, Tetrapods and Accropodes. In: Proceedings of Breakwater '88, Eastboune.